Article | Received 26 November 2024; Accepted 13 February 2025; Published 16 April 2025
https://doi.org/10.55092/esp20250002

Vibrational spectroscopy of lead-free potassium sodium niobate and related perovskite ferroelectrics

Seiji Kojima

Department of Materials Science, University of Tsukuba, Tsukuba, Ibaraki 305-8573, Japan;
E-mail: kojima@ims.tsukuba.ac.jp.

Highlights:

- Lead-free potassium sodium niobate (KNN) is one of the important piezoelectrics.
- Alkali niobates and KNN family with perovskite structure are reviewed.
- The ferroelectric instability of KNN has an order-disorder nature.
- KNN shows elastic anomalies in structural phase transitions.

Abstract: The potassium sodium niobate $(K_xNa_{1-x})NbO_3$ (KNN) family with the perovskite structure is a technologically important lead-free piezoelectric material. This paper reviews the ferroelectric and structural phase transitions of KNN and related materials. The nature of end members, the physical properties, and phase transitions of simple alkali niobate materials $MNbO_3$ (M=Li, Na, K, Rb, and Cs) are reviewed. The binary solid solution's phase diagram, KNN, is introduced concerning the morphotropic phase boundary (MPB). To understand the phase transitions near the MPB composition, the temperature dependences of lattice dynamical properties of KNN single crystals on optical modes and acoustic modes are reviewed by Raman and Brillouin scattering studies, respectively. Physical properties and phase transitions of KNN-based solid solutions were also reviewed.

Keywords: lead-free perovskite; potassium sodium niobate; morphotropic phase boundary; ferroelectric phase transition; elastic; Raman scattering; Brillouin scattering

1. Introduction

Ferroelectric materials have been extensively applied to various devices with many attractive functionalities such as pyroelectric, piezoelectric, nonlinear optic, elasto-optic effects. In 1942, the ferroelectricity instability was suggested by the anomalous dielectric response in $BaTiO_3$ [1]. It is the first piezoelectric oxide material with chemical stability. Its crystal structure is the same as a mineral perovskite ($CaTiO_3$) with a perovskite structure. Various perovskite oxide ferroelectrics have been developed and are very important in the industry.

The instability of ferroelectricity and antiferroelectricity of ABO_3 perovskite ferroelectrics was classified using the following "tolerance factor" defined by

$$t = \frac{R_A + R_O}{\sqrt{2}\,(R_B + R_O)}. \quad (1)$$

Here, R_A, R_B, and R_O denote the ionic radii of A, B, and O ions, respectively [2]. At $t = 1.0$ an ideal packing occurs. In most materials with the perovskite structure, the range of t is between 0.9 and 1.1 [3]. For $1.1 \geq t > 1.0$, there is enough space for off-center B ions related to ferroelectric behavior. At $t = 1.0$, not ferroelectricity but quantum paraelectricity appears. For $1.0 > t \geq 0.9$, a tilt of oxygen octahedra occurs by tight space of B ion in an octahedron and it induces superstructure or antiferroelectricity. Goldschmidt's tolerance factor was investigated for perovskite materials [4]. The effect of doping on the tolerance factor was also studied [5].

2. Simple alkali niobates

The niobium oxide perovskites are environmentally friendly materials and have been widely recognized because of their excellent piezoelectric, nonlinear optic, photocatalytic properties, and high-energy storage density [6]. The t factors of alkaline niobates, $MNbO_3$ (M = Li, Na, K, Rb, Cs), are $LiNbO_3$: $t = 0.75$; $NaNbO_3$: $t = 0.97$; $KNbO_3$: $t = 1.05$; $RbNbO_3$: $t = 1.09$, and $CsNbO_3$: $t = 1.14$. The tolerance factor of $LiNbO_3$ is smaller than 0.8 and its crystal structure is not the perovskite but the $LiNbO_3$ structure [7], which is similar to the ilmenite structure. The room temperature phase of $LiNbO_3$ is ferroelectric with a trigonal space group *R3c* and a Curie temperature $T_C = 1200$ °C [8]. When the t factor increases by the substitution of Li by Na, the perovskite structure is reported in $Li_{0.2}Na_{0.8}NbO_3$ crystals. A ferroelectric phase (*R3c*) was observed at ambient temperature by powder neutron diffraction [9].

The tolerance factor of $NaNbO_3$ with the perovskite structure is between 0.9 and 1.0. An antiferroelectric orthorhombic phase (point group: *mmm*) was observed at room temperature [10]. Recent Rietveld analysis by the diffraction experiments by X-ray and neutron reported that ferroelectric (space group: $P2_1ma$) phase and antiferroelectric ($Pbma$) one coexist in the temperature region 27 °C ≤ T ≤ 342 °C [11]. $NaNbO_3$ is highly polymorphic, and more than eight phases were reported in the large temperature region from −200 °C to 643 °C. Doping $(Ba_{0.7}Ca_{0.3})TiO_3$ (BCT) into $NaNbO_3$ destabilizes the antiferroelectric phase of pure $NaNbO_3$ and enhances the existence of the ferroelectric phase ($Pmc2_1$) [12].

The tolerance factor of $KNbO_3$ is more than 1.0, and it is ferroelectric with the orthorhombic point group (*mm2*) at room temperature [13]. $KNbO_3$ has received renewed interest because of the large electromechanical coupling constant for longitudinal acoustic modes and surface acoustic waves (SAWs) [14]. $KNbO_3$ undergoes the successive phase transition, which is generated by a prototypic phase and a set of degenerate soft modes [15]. The high-temperature prototypic phase is cubic ($Pm\bar{3}m$). Upon cooling tetragonal (*P4mm*), orthorhombic (*Bmm2*), and rhombohedral (*R3m*) phases successively appear. The successive phase transition of $KNbO_3$ belongs to a homophone sequence, and it is the same as that of $BaTiO_3$ with the perovskite structure.

The tolerance factor of $RbNbO_3$ is more than 1.0 and is larger than that of $KNbO_3$. It is ferroelectric with the orthorhombic point group (*mm2*) at room temperature [16]. Theoretical calculation of $RbNbO_3$ by first principles within the density functional theory predicted that

rhombohedral *R3m* is the ground-state structure [17]. However, polycrystalline $RbNbO_3$ was recently obtained by high-pressure and high-temperature (HPHT) synthesis [18]. It was found that $RbNbO_3$ undergoes a first-order tetragonal (*4mm*) to orthorhombic (*mm2*) phase transition at 519 K and there is no transition below 5 K to a rhombohedral (*3m*) phase [16]. Further study is required on the ground state and phase transitions of perovskite $RbNbO_3$. In the orthorhombic phase, spontaneous polarization was larger than that of $KNbO_3$, and this fact may be related to the larger tolerance factor than $KNbO_3$.

The tolerance factor of $CsNbO_3$ (CNO) is also larger than 1.0. The synthesis is not yet reported in our knowledge. The cubic perovskite phase was hypothesized in CNO to study the technologically important electronic, photocatalytic, elastic, and optical properties [19]. The first-principles calculation reported that $CsNbO_3$ is thermodynamically unstable at ambient pressure, though it becomes stable at 20 GPa [20]. The study by first-principles calculation reported that the A-site cations in $K_{1-x}Rb_xNbO_3$ and $K_{1-x}Cs_xNbO_3$ alloys ($0 \leq x \leq 0.75$) with polymorphic tetragonal systems have no contribution to the total Ps. For the polymorphic orthorhombic systems, Nb off-centering displacements in the NbO_6 octahedra are the main mechanism for ferroelectricity in both $K_{1-x}Rb_xNbO_3$ and $K_{1-x}Cs_xNbO_3$ alloys [21]. Since high-quality single crystals are available for $LiNbO_3$, $NaNbO_3$, and $KNbO_3$, the crystal growth is very important to study the physical properties of $RbNbO_3$ and $CsNbO_3$.

3. Solid solutions $(K_xNa_{1-x})NbO_3$ (KNN)

3.1. Successive phase transition of $KNbO_3$

A successive phase transition of $KNbO_3$ belongs to a homophone sequence, which is equivalent to the successive phase transition of $BaTiO_3$. From a high-temperature phase with cubic symmetry, it undergoes phase transitions to tetragonal, orthorhombic, and rhombohedral phases at 418, 225, and −10 °C, respectively [22]. The off-center displacement of Nb^{5+} ions can be attributed to the local pseudo-Jahn-Teller effect (PJTE) of transition metal Nb^{5+} ions in NbO_6 octahedra [23]. Both displacive and order-disorder instability were discussed in its ferroelectricity. As the diffuse nature of a ferroelectric phase transition, an intense quasi-elastic scattering was reported in an inelastic neutron scattering study [24]. The softening of an infrared active T_{1u} mode or critical slowing down toward T_C was observed above T_C by Hyper-Raman scattering [25]. The triply degenerate phonons induced the direct transition between cubic and rhombohedral phases. The intermediate cubic-tetragonal and tetragonal-orthorhombic transitions are triggered by relaxation processes in the dielectric anomaly [26].

3.2. Successive phase transition of $NaNbO_3$

$NaNbO_3$ has been widely used as an end member of the lead-free piezoelectric perovskites [27]. The number of phase transitions in $NaNbO_3$ is maximal among all the oxide perovskites. At least, seven phases were reported, from a high-temperature prototypic C ($Pm\bar{3}m$) into T_1 (*P4/mbm*), O_1 (*Ccmm*), O_2 (*Pmmn*), O_3 (*Pmnm*), O_4 (*Pbma*), and R (*R3c*) phases [28]. Weak dielectric anomalies in the temperature region from 130 °C to 190 °C indicate the possibility of an incommensurate phase. These phase transitions belong to a heterophone sequence in which the soft mode system consists of two or more different sets of degenerate modes [29]. Raman scattering spectra included many Raman active modes, and the anharmonic effect was observed [30]. Its crystal structure is still controversial, and the

coexistence of a few phases was reported at room temperature by the observation of a transmission electron microscope [31]. The stoichiometry and the vacancy generated by the evaporation of Na in the synthesis may play a dominant role in the crystal structure [32]. The effect of cationic substitutions in the A and B sublattices of the $NaNbO_3$-based piezoelectric ceramics $[(1-x)(NaNbO_3\text{-}0.1BaTiO_3)]\text{-}xBaZrO_3$ with x=0–0.05 was reported [33]. To clarify the role of A and B sublattices, further study is necessary.

3.3. Potassium sodium niobate $(K_{1-x}Na_x)NbO_3$

3.3.1. Phase diagram

Potassium sodium niobate $(K_{1-x}Na_x)NbO_3$ (KNN) piezoelectrics are important lead-free ferroelectrics with a high T_C replacing $Pb(Zr_xTi_{1-x})O_3$ (PZT) [34]. As shown in Figure 1, KNN has the perovskite structure and A sites are occupied at random by Na and K.

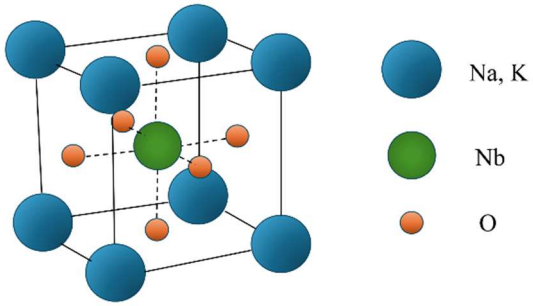

Figure 1. $(K_{1-x}Na_x)NbO_3$ with perovskite structure.

In various elements doping of KNN-based ceramics, the enhancement of the local heterogeneity in structure and average tetragonal symmetry have attracted attention to clarify the outstanding piezoelectricity [35]. KNN has a morphotropic phase boundary (MPB). It is parallel to the temperature axis on the phase diagram similar to PZT [36,37]. Figure 2 shows a comprehensive phase diagram of $K_xNa_{1-x}NbO_3$ studied by single crystal and powder X-ray diffraction [36]. Single crystals with the composition x = 0.00–0.40 were grown using the flux with solvent $NaBO_2$. Using the single crystals the dielectric anomalies were observed related to phase transitions, which had never been observed before in ceramic samples [28]. The phase diagram of the Na-rich region is not yet confirmed. The effect of the K/Na ratio on the KNN phase diagram and physical properties were studied by the sample with x = 0.48–0.54 synthesized using a standard solid-state reaction method. The typical MPB was reported at x = 0.52–0.525, which separates the monoclinic phase from the orthorhombic one [37]. Using the ceramics near x = 0.52, the best values of a piezoelectric constant d_{33} = 160 pC/N and an electromechanical coupling coefficient k_t = 47% were observed. The K-rich region with the composition $0.525 < x \leq 1.0$, the successive phase transition from a prototypic cubic ($m\bar{3}m$) to tetragonal (*4 mm*), orthorhombic (*mm2*), and rhombohedral (*3m*) phases occurs as same as that of $KNbO_3$. By the sol-gel synthesis of K-rich KNN the existence of K-rich phase was reported by energy-dispersive X-ray spectroscopy [38].

The phase diagram of KNN has a similarity to that of $Pb(Zr_xTi_{1-x})O_3$ (PZT) [39]. In both solid solutions one end member is ferroelectric and another end member is antiferroelectric. MPBs of PZT and KNN are nearly parallel to the temperature axis, and this fact is very important for the piezoelectric application because of the very small temperature variation of dielectric and piezoelectric properties. The

tolerance factor of $K_{0.5}Na_{0.5}NbO_3$ (KNN50) is 1.01, which may indicate the frustration between ferroelectric and antiferroelectric interactions. The composition is slightly smaller than that of MPB composition, at which monoclinic and orthorhombic phases coexist and the structural phase transitions become complicated. In the following section, the dynamical properties of structural phase transitions of KNN50 are discussed based on Raman and Brillouin scattering studies.

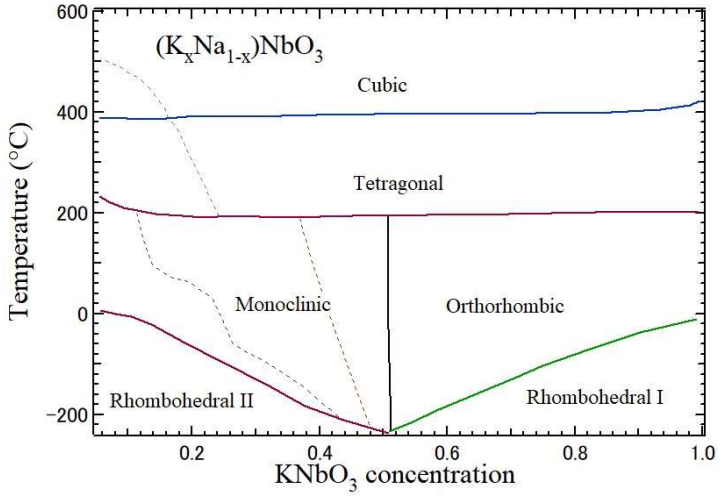

Figure 2. Phase diagram of $K_xNa_{1-x}NbO_3$. A morphotropic phase boundary (MPB) is found at the concentration x = 0.52–0.525.

3.3.2. Lattice instability of KNN50

The lattice dynamical properties were investigated in phase transitions of KNN50 by Raman scattering [40]. The flux-grown crystals undergo a phase transition from cubic ($m\bar{3}m$) to ferroelectric tetragonal (*4mm)* phases at T_C = 430 ºC, and the tetragonal to monoclinic (m) phase transition at T_{tm} = 190 ºC [41]. The composition measured by the inductively coupled plasma emission spectroscopy was $K_{0.47}Na_{0.53}NbO_3$. The Raman spectra between 10 and 1000 cm^{-1} at several temperatures are shown in Figure 3. In most perovskite oxides, Raman active modes appear in the frequency region below 1000 cm^{-1}. In a cubic phase with a point group $m\bar{3}m$, there is no Raman active mode. However, the broad peaks appear at about 250 and 580 cm^{-1}, and such peaks are originated from the local symmetry breaking by polar nano regions (PNRs) [42]. Upon cooling from a cubic paraelectric phase (C), peaks at ν_3, ν_6, and ν_7 appear in a tetragonal phase (T). Upon further cooling from a tetragonal phase, the peaks of ν_1, ν_2, ν_4, and ν_5 appear in a monoclinic phase (M).

In the monoclinic phase, the low-frequency mode (ν_1) at 68 cm^{-1} and room temperature is attributed to the lattice mode related to the displacement of a structural phase transition. The high-frequency modes are internal modes [43]. The mode (ν_3) at about 260 cm^{-1} is assigned to the bending mode of a NbO_6 octahedron. The peak (ν_6) at about 630 cm^{-1} and its shoulder peak (ν_5) at ~570 cm^{-1} are assigned to the stretching vibration of NbO_6 octahedra. The high-frequency mode (ν_7) at about 870 cm^{-1} is assigned to the coupled mode of bending and stretching modes of NbO_6 octahedra. These internal modes are common in perovskite oxides and are sensitive to local distortions. In $KNbO_3$, the variation of these modes was discussed among tetragonal, orthorhombic, and rhombohedral phases [44]. In Figure 3, the splitting of the stretching mode at about 600 cm^{-1} (ν_6) in the cubic phase occurs upon cooling into tetragonal and monoclinic phases. The enhancement of the splitting is attributed to the increase of local

distortion of NbO_6 octahedra. The bending mode at about 260 cm^{-1} in the tetragonal phase shows softening upon cooling down to the monoclinic phase and upon further cooling hardening occurs.

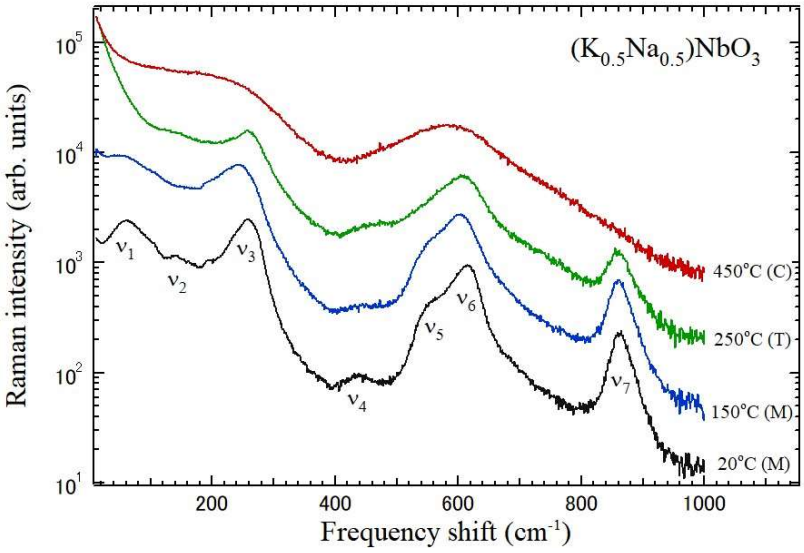

Figure 3. Raman scattering spectra of a KNN50 crystal at several temperatures. C, T, and M denote cubic, tetragonal, and monoclinic phases, respectively.

Below the Curie temperature, the lattice instability of a tetragonal to monoclinic phase transition was studied by the external modes in Raman scattering below 200 cm^{-1} [40]. On heating from room temperature, the frequency of the lowest underdamped peak at 68 cm^{-1} shows gradual softening as shown in Figure 4. Its width increases markedly and becomes overdamped towards T_{tm} = 190 ºC by the strong anharmonicity.

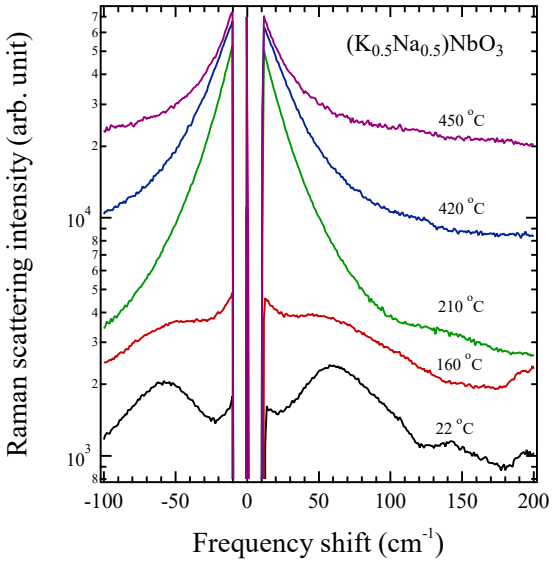

Figure 4. Low-frequency Raman spectra of a KNN50 crystal at selected temperatures.

Figure 5 shows the temperature dependence of the lowest mode frequency and damping factor. It indicates the crossover in the tetragonal-monoclinic phase transition from a displacive nature to order-disorder nature. The order-disorder nature was clearly observed in Figure 4. For further heating from T_{tm} in a tetragonal phase, the strong central peak (CP) is observed just above T_{tm}. The intensity of a

CP becomes maximum at T_C. The relaxation time calculated by the CP width increases upon heating and the critical slowing down was observed towards T_C [40].

For further heating, the broad CP was observed just above T_{tm}. The CP intensity gradually becomes weak as shown in Figure 5. Usually, a CP was observed by inelastic light scattering such as Raman and Brillouin scattering. As the origins of CPs, several different mechanisms were discussed. Whether the origin of CP is static or dynamic is very important. The static one is attributed to a relatively narrow temperature-independent and elastic CP. In contrast, the dynamic one is attributed to a temperature-dependent and relatively broad CP. The distinctions between various dynamic origins are discussed by their symmetry, temperature, and wave vector dependence. The origin of CP is attributed to the polarization fluctuation in a ferroelectric phase transition [45]. The relaxation time of polarization fluctuations is calculated by the CP width [46,47]. The reciprocal relaxation time and the temperature divided by a CP intensity are shown as a function of temperature in Figures 6 and 7, respectively. Upon heating from T_{tm}, the reciprocal relaxation time increases at first. However, above 350 °C the reciprocal relaxation time reaches a sharp minimum at T_C. It is the evidence of a critical slowing down near T_C. Such a slowing down suggests that the order-disorder nature can be caused by the eight-site model of Nb^{5+} off-center along the [111] direction at B-site [48], which is also predicted for $KNbO_3$ by the pseudo-Jahn-Teller model [49]. The CP intensity becomes strong in a tetragonal phase with *P4mm* symmetry, because the CP is Raman active below T_C. However, the CP decreases remarkably above T_C. The polarization fluctuations related to the CP are Raman inactive in $Pm\bar{3}m$ symmetry. The weak CP intensity may have originated from the local symmetry breaking by polar nanoregions (PNRs). By the same mechanism, Raman modes near 250 and 600 cm^{-1} appear above T_C.

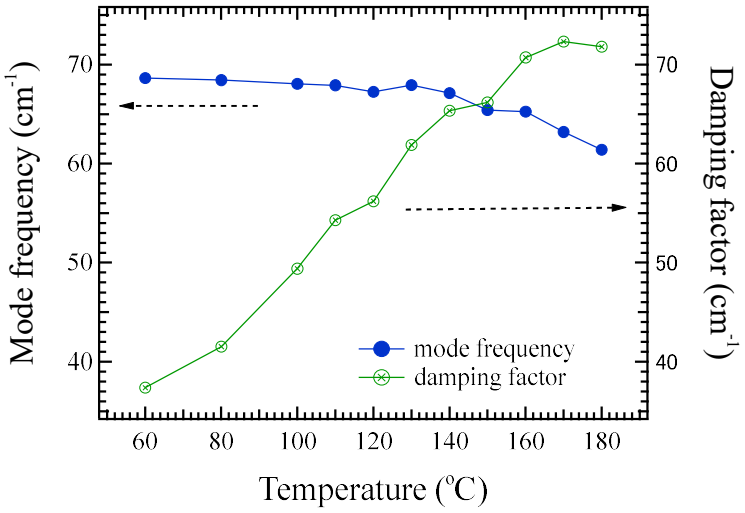

Figure 5. The soft mode frequency and damping factor of a KNN50 crystal are shown as a function of temperature.

In a second order phase transition, the temperature dependence of relaxation time related to the critical slowing down is given by the following equation in the vicinity of T_C,

$$\frac{1}{\tau_{CP}} = \frac{1}{\tau_0} + \frac{1}{\tau_1}\left(\frac{T-T_C}{T_C}\right) \quad , \quad (T>T_C). \tag{2}$$

where τ_0 and τ_1 are the constants. In a first order phase transition, the reciprocal relaxation time is given by the following equation:

$$\frac{1}{\tau_{CP}} = \frac{1}{\tau_0} + \frac{1}{\tau_1}\left(\frac{T-T_1}{T_1}\right) \quad , \quad (T>T_C>T_1). \tag{3}$$

In a cubic to tetragonal phase transition of a KNN50 crystal at T_C = 430 °C, the relaxation time is plotted as a function of temperature as shown in Figure 6. The observed values of the fitting parameters are τ_0 = 3.95 ps, τ_1 = 1.21 ns, and T_1 = 389.5 °C. The slowing down towards T_C can be clear evidence of the order-disorder nature in a ferroelectric phase transition with the off-center Nb ions.

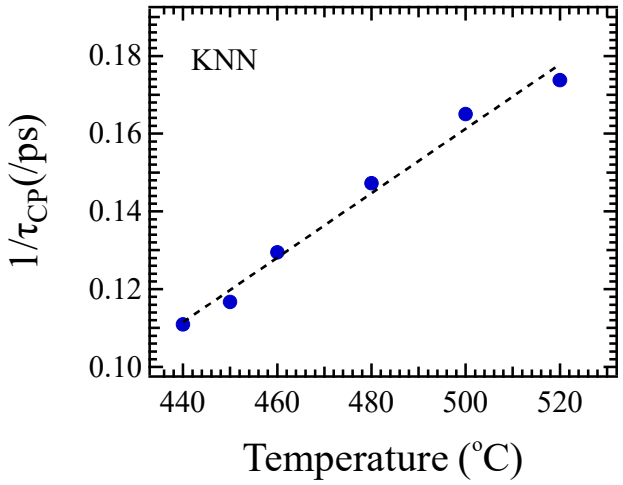

Figure 6. The reciprocal relaxation time calculated by the CP width is plotted as a function of temperature.

The intensity of a central peak I_{CP} for a first-order phase transition obeys the following equation above T_C [43]:

$$\frac{T}{I_{CP}} \propto \left(\int_0^\infty \frac{\chi''(\omega)}{\omega} d\omega\right)^{-1} \propto \frac{1}{\chi'(0)} = \frac{T-T_1}{C}, \quad (T>T_C>T_1). \tag{4}$$

Figure 7 shows T/I_{CP} of a KNN50 crystal as a function of temperature. The observed fitting parameters are C = 3.51 × 10^{-4} and T_1 = 389.5 °C. Since the inverse static dielectric constant $1/\chi'(0)$ is proportional to the square of the soft mode frequency according to the Lyddane–Sachs–Teller relation, such a Curie-Weiss behavior may indicate the displacive ferroelectric instability.

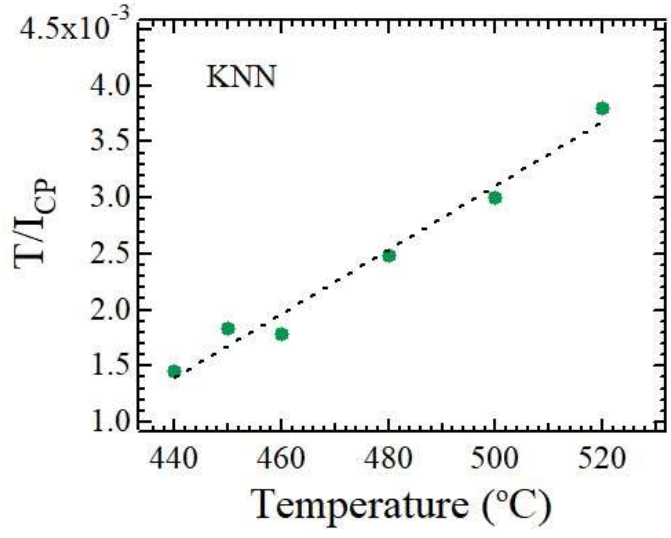

Figure 7. Temperature dependence of the temperature divided by a central peak intensity I_{CP}.

3.3.3. Elastic anomalies

The temperature-dependent elastic properties and related relaxation process of KNN50 crystals were studied by broadband Brillouin scattering, which is a powerful non-contact method to measure sound velocity and dynamics in a GHz range [50]. The temperature-dependent Brillouin scattering of a KNN50 crystal was studied as shown in Figure 8 [51]. The doublet peaks of a longitudinal acoustic (LA) mode appeared at ± 64 GHz and 50 °C. The doublet peaks of a transverse acoustic (TA) mode also appeared at ± 34 GHz and 50 °C. The difference in the peak height between LA and TA modes is attributed to the difference in photoelastic constants between LA and TA modes [52].

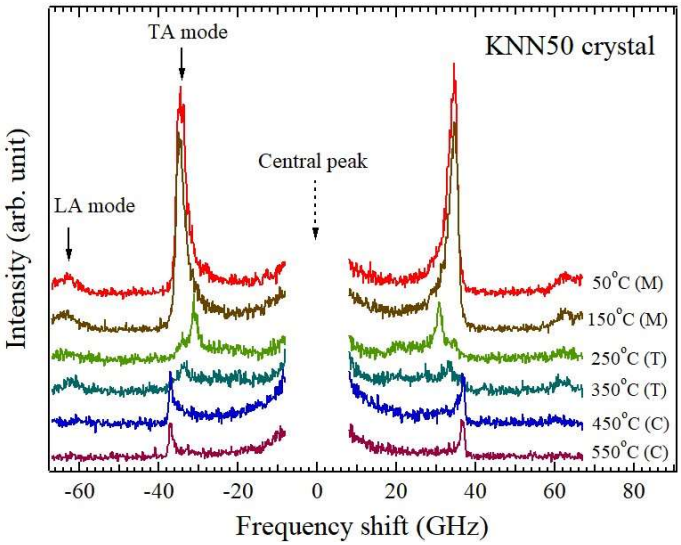

Figure 8. Brillouin scattering spectra of a KNN50 crystal observed in a backward scattering geometry as a function of temperature. Both TA and LA peaks appeared.

The frequency shift ν_B is related to sound velocity V of a sample by the following equation:

$$V = \frac{\lambda_i \nu_B}{2\, n \sin\frac{\theta}{2}}, \quad (5)$$

where, λ_i, θ, and *n* are the wavelength of an incident laser beam, the scattering angle between the incident and scattered light, and the refractive index of a sample at λ_i, respectively. The LA velocity V_{LA} and TA velocity V_{TA} were determined from the LA and TA frequency shifts, respectively. The elastic stiffness constants c_{11} and c_{44} in pseudo-cubic coordinates are calculated from V_{LA} and V_{TA}, respectively, by the following equations:

$$c_{11} = \rho V_{LA}^2, \quad c_{44} = \rho V_{TA}^2, \quad (6)$$

where $\rho = 4.506$ g/cm^3 is the density [53]. Figure 9 shows elastic constants c_{11}, c_{44} of a KNN crystal as a function of temperature. The values of $c_{11} = 232$ GPa, and $c_{44} = 69.7$ GPa at room temperature are close to $c_{11} = 226$ GPa, and $c_{44} = 74.3$ GPa of $KNbO_3$ at 25 °C [54]. The partial softening of c_{11} and c_{22} was observed in the vicinity of T_C and T_{tm}, respectively, which is related to the structural changes.

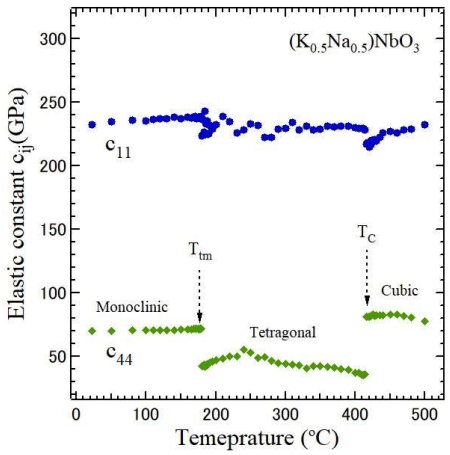

Figure 9. Elastic stiffness constants c_{11} and c_{44} of a KNN50 crystal as a function of temperature.

4. Physical properties of KNN based ceramics

As the promising lead-free piezoelectrics, KNN-based ceramics have been extensively studied [55–57]. In PZT, piezoelectric and dielectric properties are markedly enhanced around an MPB. Since MPB plays a dominant role in large piezoelectricity, the investigation of a phase diagram is important. The phase diagrams of the binary $(1-x)(K_{0.5}Na_{0.5})NbO_3$-$xMTiO_3$ (M = Pb, Ba, Sr, Ca, and $Bi_{0.5}Li_{0.5}$) solid solutions were studied over a broad temperature range of 10 K ≤ T ≤ 770 K. In the $(1-x)(K_{0.5}Na_{0.5})NbO_3$-$xSrTiO_3$ ($(1-x)$KNN-xST) solid solution, the piezoelectric constant of 0.95NKN-0.05ST was found as high as 190 pC/N [56,58]. To confirm the appearance of the tetragonal phases in a phase diagram, the Raman scattering spectra of 0.975KNN-0.025ST at 100 °C and 0.9KNN −0.1ST at 23 °C were measured [58]. Figure 10 shows the Raman spectrum of 0.9KNN-0.1ST at 23 °C in a tetragonal phase. Three peaks (ν_3, ν_6, and ν_7) were observed and the appearance of these peaks is the same as those of the tetragonal phase of a $(K_{0.5}Na_{0.5})NbO_3$ crystal at 250 °C shown in Figure 3. From the shape of their spectra, the crystal symmetry of a phase was determined to be tetragonal. Variations of Raman scattering spectra of $(1-x)$KNN-xST ceramics were measured to investigate the crystal symmetry in a phase diagram [59]. The temperature dependence of the $CaTiO_3$-modified $(K_{0.5}Na_{0.5})NbO_3$ system was also measured by Raman scattering [58]. Raman scattering spectra are very sensitive to crystal structures and can be a powerful tool to investigate their crystal structures.

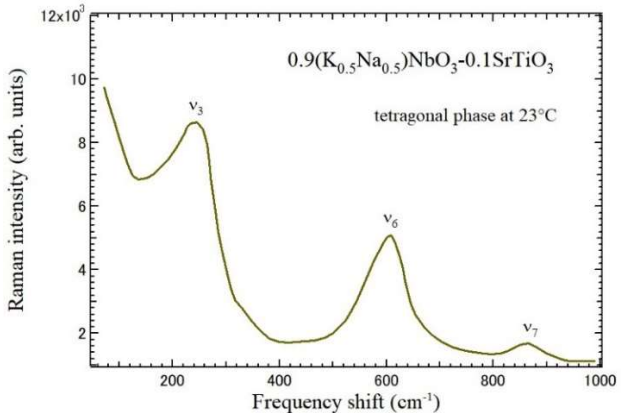

Figure 10. Raman scattering spectrum of $0.9(K_{0.5}Na_{0.5})NbO_3$-$0.1SrTiO_3$ (0.9KNN-0.1ST) in a tetragonal phase at 23 °C.

The MPB was also studied in ternary $(1-x-y)(K_{0.5}Na_{0.5})NbO$-$xBZrO_3$-$yATiO_3$ solid solutions when $0.08 \leq x+y \leq 0.10$ [60]. When $ATiO_3$ (A = Sr, Ba, Ca, Pb, etc.) is mixed into $(K_{0.5}Na_{0.5})NbO_3$, a tetragonal phase appears at room temperature [61,62]. While, when $BZrO_3$ (B = Ca, Sr, Ba,) is mixed into $(K_{0.5}Na_{0.5})NbO_3$, the rhombohedral phase appears at room temperature. Consequently, the MPB between tetragonal and rhombohedral phases is formed at room temperature by mixing $ATiO_3$ and $BZrO_3$ into $(K_{0.5}Na_{0.5})NbO_3$. $(K_{0.5}Na_{0.5})NbO_3$- $BaZrO_3$- $(Bi_{0.5}M_{0.5})TiO_3$ (M = Li, K) piezoelectric ceramics were also studied on the temperature dependences of dielectric constant, piezoelectric d_{33} constant, electromechanical coupling coefficient, and Raman spectra [61,62]. For the formation of the MPB, two end members, one with a tetragonal phase and the other with a rhombohedral phase at room temperature, are necessary. $(1-x)(K_{0.5}Na_{0.5})NbO_3$-$xBaZrO_3$ has a rhombohedral symmetry ($0.08 \leq x \leq 0.15$) and $(1-x)$—$(K_{0.5}Na_{0.5})NbO_3$-$x(Bi_{0.5}Li_{0.5})TiO_3$ has a tetragonal symmetry ($0.06 \leq x \leq 0.15$) at room temperature. Therefore, by incorporating $BaZrO_3$ and $(Bi_{0.5}Li_{0.5})TiO_3$ into $(K_{0.5}Na_{0.5})NbO_3$, the formation of an MPB is possible. Figure 11 shows Raman scattering spectra of $0.92(K_{0.5}Na_{0.5})NbO_3$-$0.07BaZrO_3$-$0.01(Bi_{0.5}K_{0.5})TiO_3$ ceramics as a function of temperature in cubic and tetragonal phases.

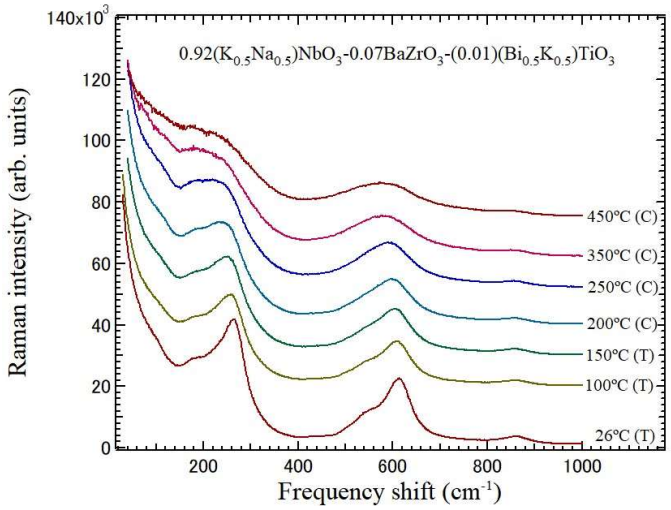

Figure 11. Raman scattering spectra of $0.92(K_{0.5}Na_{0.5})NbO_3$-$0.07BaZrO_3$-$0.01(Bi_{0.5}K_{0.5})TiO_3$ ceramics at selected temperatures. C and T denote cubic and tetragonal phases, respectively.

The stretching mode of oxygen octahedra is sensitive to the distortion of octahedra and splitting occurs in a tetragonal symmetry. Figure 12 shows the mode frequency of stretching modes of $0.92(Na_{0.5}K_{0.5})NbO_3$-$0.07BaZrO_3$-$0.01(Bi_{0.5}K_{0.5})TiO_3$ ceramics at selected temperatures. The splitting of stretching mode frequency was observed below the cubic to tetragonal phase transition temperature [63].

In a recent study on Sm-modified $(K_{0.5}Na_{0.5})NbO_3$, the effect of Sm-doping was investigated by Raman scattering [64]. It was suggested that the substitution of heavier Sm ions with lighter K/Na ions confirms the A-site occupancy of the Sm ions in Sm-modified $(K_{0.5}Na_{0.5})NbO_3$ ceramics. The composition-dependent physical properties and related structural phase transitions were also studied in $CaTiO_3$-modified $K_{0.5}Na_{0.5}NbO_3$ and $(1-x)(K_{0.5}Na_{0.5})NbO_3$-$x(Ba_{0.5}Sr_{0.5})TiO_3$ solid solutions [57,65]. Raman scattering spectroscopy is also useful to investigate the site occupancy of the doped ions.

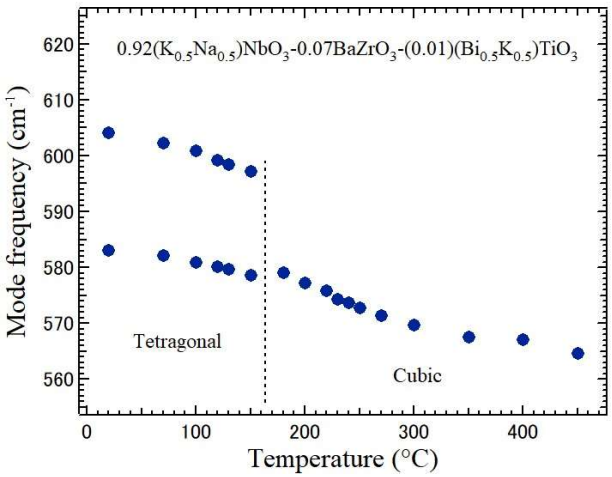

Figure 12. Temperature dependence of mode frequency of stretching modes of $0.92(K_{0.5}Na_{0.5})NbO_3$-$0.07BaZrO_3$-$0.01(Bi_{0.5}K_{0.5})TiO_3$ system. The splitting of mode frequency occurs below the Curie temperature.

5. Conclusions

As a typical lead-free piezoelectric material, ferroelectric and structural phase transitions of potassium sodium niobate $(K_xNa_{1-x})NbO_3$ (KNN) family with the perovskite structure were reviewed in the viewpoint of vibrational spectroscopy. The phase transitions and physical properties of simple alkali niobate materials $MNbO_3$ (M=Li, Na, K, Rb, and Cs) are introduced. Ferroelectric and structural phase transitions of their binary KNN solid solutions are described with the morphotropic phase boundary (MPB). The lattice instability and elastic properties in structural phase transitions are discussed on KNN crystals by Raman and Brillouin scattering spectroscopies, respectively. Raman scattering also studied the physical properties and phase boundaries of KNN-based solid solutions.

Conflicts of interests

The author declares no conflict of interest.

References

[1] Wainer E, Salmon AN. Titanium Alloy Mfg. *Co. Elect Rep*. 1942, 8.
[2] Goldschmidt VM. Die Gesetze der Krystallochemie. *Naturwissenschaften* 1926, 14(21):477–485.
[3] Xu Y. *Ferroelectric Materials and Their Applications*, Amsterdam: North-Holland, 1991, pp.101–103.
[4] Tidrow SC. Mapping Comparison of Goldschmidt's Tolerance Factor with Perovskite Structural Conditions. *Ferroelectrics* 2014, 470(1):13–27.
[5] Devi CS, Omprakash J, Malathi AR, Kumar GS, Prasad G. Influence of distortions and tolerance factor on the structure of ABO_3 type perovskites and complex perovskites, *Ferroelectrics* 2020, 554(1):172–186.

[6] Qi H, Zuo R, Xie A, Tian A, Fu J, *et al.* Ultrahigh Energy-Storage Density in $NaNbO_3$-Based Lead-Free Relaxor Antiferroelectric Ceramics with Nanoscale Domains. *Adv. Funct. Mater.* 2019, 29(35):1903877.

[7] Abrahams SC, Levinstein HJ, Reddy JM. Ferroelectric lithium niobate. 5. Polycrystal X-ray diffraction study between 24° and 1200 °C. *J. Phys. Chem. Solids* 1966, 27(6–7):1019–1026.

[8] Nassau K, Levinstein HJ. Ferroelectric behavior of lithium niobate. *Appl. Phys. Lett.* 1965, 7(3):69–70.

[9] Dixon CAL, McNulty JA, Huband S, Thomas PA, Lightfoot P. Unprecedented phase transition sequence in the perovskite $Li_{0.2}Na_{0.8}NbO_3$. *IUCrJ.* 2017, 4(3):215–222.

[10] Wells M, Megaw HD. The Structures of $NaNbO_3$ and $Na_{0.975}K_{0.025}NbO_3$. *Proc. Phys. Soc. (London)* 1961, 78(6):1258–1259.

[11] Htet CS, Nayak S, Manjón-Sanz A, Liu J, Kong J, *et al.* Atomic structural mechanism for ferroelectric-antiferroelectric transformation in perovskite $NaNbO_3$. *Phys. Rev. B* 2022, 105(7):174113.

[12] Wajhal S, Mishra SK, Shinde AB, Krishna PSR, Mittal R. Role of correlated disorder on structural stability and functional properties in (Na,Ba)(Nb,Ti)O_3. *J. Alloys and Compounds* 2021, 866(15):158982.

[13] Shirane G, Danner H, Pavlovic A. Pepinsky R. Phase Transitions in Ferroelectric $KNbO_3$. *Phys. Rev*. 1954, 93(4):672–673.

[14] Nakamura K. *Potassium Niobate ($KNbO_3$) Crystals and Their applications*. Trolier-Mckinstry S, Cross LE, Yamashita Y, Eds. Piezoelectric Single Crystals and Their Application; University Park, PA, USA: Susan Trolier-McKinstry, 2004, pp.377–395.

[15] Aizu K. General Considerations of Homophone Sequences of Phase Transitions. *J. Phys. Soc. Jpn.* 1975, 38(6):1592–1600.

[16] Fukuda M, Yamaura K. Experimental studies on crystal structures and phase transitions in perovskite-type $RbNbO_3$. *J. Cer. Soc. Jpn*. 2023, 131(5):126–129.

[17] Lebedev AI. Ferroelectric properties of $RbNbO_3$ and $RbTaO_3$. *Phys. Solid State* 2015, 57(2):331–336.

[18] Yamamoto A, Murase K, Sato T, Sugiyama K, Kawamata T, *et al.* Crystal structure and properties of perovskite-type rubidium niobate, a high-pressure phase of $RbNbO_3$. *Dalton Trans.* 2024, 53(16):7044–7052.

[19] Monira M, Helal MA, Liton MNH, Kamruzzaman M, Kojima S. Elastic, optoelectronic and photocatalytic properties of semiconducting $CsNbO_3$: first principles insights. *Sci. Rep.* 2023, 13(1):10246.

[20] Monira M, Liton MNH, Al-Helal M, Kamruzzaman M, Ul Isla AKMF, *et al.* Acoustic and thermodynamic properties of cesium niobate under pressure and temperature: A DFT study. *Open Ceram.* 2024, 17:100546.

[21] Oh SV, Hwang W, Kim K, Lee J, Soon A. Using Feature-Assisted Machine Learning Algorithms to Boost Polarity in Lead-Free Multicomponent Niobate Alloys for High-Performance Ferroelectrics. *Adv. Sci.* 2022, 9(13):2104569.

[22] Wood EA. Polymorphism in potassium niobate, sodium niobate, and other ABO_3 compounds. *Acta Crystallogr*. 1951, 4(4):353–362.

[23] Bersuker IB. Polinger V. Perovskite Crystals: Unique Pseudo-Jahn–Teller Origin of Ferroelectricity, Multiferroicity, Permittivity, Flexoelectricity, and Polar Nanoregions. *Condens. Matter* 2020, 5(4):68.

[24] Nunes AC, Axe JD, Shirane G. A neutron study of diffuse scattering in cubic $KNbO_3$. *Ferroelectrics* 1971, 2(1):291–297.

[25] Vogt H, Fontana MD, Kugel GE, Günter P. Low-frequency dielectric response in cubic $KNbO_3$ studied by hyper-Raman scattering. *Phys. Rev.* 1986, 34(1):410–415.

[26] Fontana MD, Ridah A, Kugel GE, Carabatos-Nedelec C. The intrinsic central peak at the structural phase transitions in $KNbO_3$. *J. Phys. C: Solid State Phys.* 1988, 21(34): 5853–5879.

[27] Wang XB, Shen ZX, Hu ZP, Qin L, Tang SH, *et al.* High temperature Raman study of phase transitions in antiferroelectric $NaNbO_3$. *J. Mol. Struc*. 1996, 385(1):1–6.

[28] Raevskii IP, Reznichenko LA, Ivliev MP, Smotrakov VG, Eremkin VV, *et al.* Growth and study of single crystals of (Na, K)NbO_3 solid solutions. *Crystallogr. Reports* 2003, 48(3):486–490.

[29] Aizu K. General Considerations of Heterophone Sequences of Transitions. *J. Phys. Soc. Jpn*. 1977, 42(2):424–432.

[30] Lima RJC, Freire PTC, Sasaki JM, Ayala AP, Melo FEA, *et al.* Temperature-dependent Raman scattering studies in $NaNbO_3$ ceramics. *J. Raman Spectrosc.* 2002, 33(8):669–674.

[31] Chen J, Feng D. TEM study of phases and domains in $NaNbO_3$ at room temperature. *Phys. Stat. Sol*. (a). 1988, 109(1):171–185.

[32] Arioka T, Taniguchi H, Itoh M, Oka K, Wang R, *et al.* Ferroelectricity in $NaNbO_3$: Revisited. *Ferroelectrics* 2010, 401(1):51–55.

[33] Politova ED, Kaleva GM, Mosunov AV, Sadovskaya NV, Fortalnova EA, *et al.* Structure, microstructure, and functional properties of modified sodium niobate ceramics. *Ferroelectrics* 2024, 618(6):1422–1430.

[34] Zhengfa L, Yongxiang L, Jiwei Z. Grain growth and piezoelectric property of KNN-based lead-free ceramics. *Curr. Appl. Phys*. 2011, 1(3):S2–S13.

[35] Gao X, Cheng Z, Chen Z, Liu Y, Meng X, *et al.* The mechanism for the enhanced piezoelectricity in multi-elements doped (K,Na)NbO_3 ceramics. *Nat. Commun.* 2021, 12(1):881.

[36] Baker DW, Thomas PA, Zhang N, Glazer AM. A comprehensive study of the phase diagram of $K_xNa_{1-x}NbO_3$. *Appl. Phys. Lett*. 2009, 95(9):091903.

[37] Dai Y, Zhang X, Chen K. Morphotropic phase boundary and electrical properties of $K_{1-x}Na_xNbO_3$ lead-free ceramics. *Appl. Phys. Lett*. 2009, 94(4):042905.

[38] Deol RS, Mehra M, Mitra B, Singh M. Low-temperature solution-processed sol-gel K-rich KNN thin films for flexible electronics. *MRS Advances* 2018, 3(5):269–275.

[39] Jaffe B, Roth RS, Marzullo S. Piezoelectric Properties of Lead Zirconate-Lead Titanate Solid-Solution Ceramics. *J. Appl. Phys*. 1954, 25(6):809–810.

[40] Kojima S, Zushi J, Noguchi Y, Miyayama M. Successive phase transition of lead-free ferroelectric sodium potassium niobate crystals studied by Raman scattering. *Ferroelectrics* 2018, 532(1):183–189.

[41] Kizaki Y, Noguchi Y, Miyayama M. Defect control for low leakage current in $K_{0.5}Na_{0.5}NbO_3$ single crystals. *Appl. Phys. Lett*. 2006, 89(14):142910.

[42] Pugachev AM, Kovalevskii VI, Surovtsev N V, Kojima S, Prosandeev SA, *et al.* Broken Local Symmetry in Paraelectric $BaTiO_3$ Proved by Second Harmonic Generation. *Phys. Rev. Lett*. 2012, 108(24):247601.

[43] Hayes W, Loudon R. *Scattering of light by crystals*. Mineola, New York: Dover Publishing, 1978, pp. 103–107.

[44] Baier-Saip JA, Ramos-Moor E, Cabrera AL. Raman study of phase transitions in $KNbO_3$. *Solid State Commun.* 2005, 135(6):367–372.

[45] Jiang F, Kojima S. Relaxation mode in 0.65PMN-0.35PT relaxor single crystals studied by micro-Brillouin scattering. *Phys. Rev. B* 2000, 62(13):8572.

[46] Pugachev AM, Anwar H, Kojima S. Order-disorder nature of lithium tantalate probed by broadband Brillouin scattering spectroscopy. *Phys. stat. sol.* (c) 2004, 1(11):3122–3125.

[47] Hushur A, Gvasaliya S, Roessli B, Lushnikov S, Kojima S, *et al.* Ferroelectric phase transition of stoichiometric lithium tantalate studied by Raman, Brillouin, and neutron scattering. *Phys. Rev. B* 2007, 76(6):064104.

[48] Comes R, Lambert M, Guinier A. The Chain Structure of $BaTiO_3$ and $KNbO_3$. *Solid State Commun*. 1968, 6(10):715–719.

[49] Polinger V. Off-center instability of Nb^{5+} in $KNbO_3$ under ambient pressure. *Chem. Phys. 2015,* 459:72–80.

[50] Kojima S. 100th Anniversary of Brillouin Scattering: Impact on Materials Science. *Materials (Basel).* 2022, 15(10):3518.

[51] Kojima S, Tsukada S, Noguchi Y. Order-disorder nature and elastic anomaly of successive phase transition of $(K_{0.5}Na_{0.5})NbO_3$ proved by broadband Brillouin scattering. *Ferroelectrics* 2022, 586(1):2–9.

[52] Vacher R, Boyer L. Brillouin scattering: A tool for the measurement of elastic and photoelastic constants. *Phys. Rev. B* 1972, 6(2):639–673.

[53] Maeda T, Takiguchi N, Ishikawa M, Hemsel T, Morita T. $(K,Na)NbO_3$ lead-free piezoelectric ceramics synthesized from hydrothermal powders. *Mater. Lett.* 2010, 64(2):125–128.

[54] Wiesendanger E. Dielectric, mechanical and optical properties of orthorhombic $KNbO_3$. *Ferroelectrics* 1974, 6(1):263–281.

[55] Saito Y, Takao H, Tani T, Nonoyama T, Takatori K, *et al.* Lead-free piezoceramics. *Nature* 2004, 432(7013):84–87.

[56] Wang R, Bando H, Itoh M. Universality in phase diagram of $(K,Na)NbO_3$–$MTiO_3$ solid solutions. *Appl. Phys. Lett*. 2009, 95(9):092905.

[57] Sahoo S, Pradhan DK, Kumari S, Sahu A, Samantaray KS, *et al.* Studies on the compositional dependent structural and electrical properties of $CaTiO_3$-modified $K_{0.5}Na_{0.5}NbO_3$ piezoelectric system. *J. Appl. Phys.* 2024, 135(24):244101.

[58] Sasanuma K, Tsukada S, Kano J, Kojima S, Wang R, *et al.* Investigation on dielectric and piezoelectric properties of $(1-x)(Na_{0.5}K_{0.5})NbO_3$-$xSrTiO_3$ ceramics. *Ferroelectrics* 2007, 348(1):508–514.

[59] Kano J, Sasanuma K, Tsukada S, Kojima S, Wang R, *et al.* Piezoelectric $(Na_{0.5}K_{0.5})NbO_3$-$SrTiO_3$ Ceramics in the Tetragonal-Orthorhombic Phase Boundary Studied by Raman Spectroscopy. *Ferroelectrics* 2007, 347(1):55–59.

[60] Wang R, Bando H. Piezoelectric ceramics and piezoelectric, dielectric, and pyroelectric devices. International Patent No. WO2008/143160. 12 Nov. 2008.

[62] Ariizumi T, Zushi J, Kojima S, Wang R, Bando H. Effects of Mn Additive on Dielectric and Piezoelectric Properties of $(Na_{0.5}K_{0.5})NbO_3$–$BaZrO_3$–$(Bi_{0.5}K_{0.5})TiO_3$ Ternary System. *Jpn. J. Appl. Phys.* 2012, 51(7S):07GC01.

[63] Zushi J, Ariizumi T, Kojima S, Wang R, Bando H. Formation of Morphotropic Phase Boundary in $(Na_{0.5}K_{0.5})NbO_3$–$BaZrO_3$–$(Bi_{0.5}Li_{0.5})TiO_3$ Lead-Free Piezoelectric Ceramics. *Jpn. J. Appl. Phys.* 2013, 52(7S):07HB02.

[64] Sahoo S, Pradhan DK, Kumari S, Samantaray KS, Singh C, *et al.* Structural heterogeneity induced enhancement of physical properties in Sm-modified $K_{0.5}Na_{0.5}NbO_3$. *J. Am. Ceram. Soc.* 2024, 107(5):3180–3193.

[65] Sahoo S, Pradhan DK, Kumari S, Samantaray KS, Singh C, *et al.* Compositional induced structural phase transitions in $(1-x)(K_{0.5}Na_{0.5})NbO_3$–$x(Ba_{0.5}Sr_{0.5})TiO_3$ ferroelectric solid solutions. *Sci. Rep.* 2023, 13(1):19096.